The EMBO Journal (2009) 28, 193–204 | © 2009 European Molecular Biology Organization | All Rights Reserved 0261-4189/09
www.embojournal.org

THE EMBO JOURNAL

RodZ (YfgA) is required for proper assembly of the MreB actin cytoskeleton and cell shape in *E. coli*

Felipe O Bendezú[1], Cynthia A Hale, Thomas G Bernhardt[2] and Piet AJ de Boer*

Department of Molecular Biology and Microbiology, School of Medicine, Case Western Reserve University, Cleveland, OH, USA

The bacterial MreB actin cytoskeleton is required for cell shape maintenance in most non-spherical organisms. In rod-shaped cells such as *Escherichia coli*, it typically assembles along the long axis in a spiral-like configuration just underneath the cytoplasmic membrane. How this configuration is controlled and how it helps dictate cell shape is unclear. In a new genetic screen for cell shape mutants, we identified RodZ (YfgA) as an important transmembrane component of the cytoskeleton. Loss of RodZ leads to misassembly of MreB into non-spiral structures, and a consequent loss of cell shape. A juxta-membrane domain of RodZ is essential to maintain rod shape, whereas other domains on either side of the membrane have critical, but partially redundant, functions. Though one of these domains resembles a DNA-binding motif, our evidence indicates that it is primarily responsible for association of RodZ with the cytoskeleton.

The EMBO Journal (2009) **28,** 193–204. doi:10.1038/emboj.2008.264; Published online 11 December 2008
Subject Categories: cell & tissue architecture; microbiology & pathogens
Keywords: MreC; MreD; PBP2; RodA; FtsZ

Introduction

Bacterial MreB actin has been implicated in cell shape maintenance, chromosome segregation and cell polarization events in a variety of rod-shaped species, including the well-studied model organisms *Bacillus subtilis*, *Caulobacter crescentus* and *Escherichia coli*. The shape of most bacterial cells is dictated by the shape of the murein (peptidoglycan) sacculus, in essence a giant and dynamic cell-shaped molecule that surrounds the entire cytoplasmic membrane. How, despite often considerable turgor pressure, non-coccal organisms manage to mould and maintain this molecule in a particular shape is an unsolved and intensely studied issue (for reviews, see Shih and Rothfield, 2006; Cabeen and Jacobs-Wagner, 2007; den Blaauwen *et al*, 2008).

The MreB protein of *E. coli* is the only known actin in the cell and, as in other species, accumulates just underneath the cytoplasmic membrane in a spiral/banded-like pattern along the long axis of the cell (Jones *et al*, 2001; van den Ent *et al*, 2001; Kruse *et al*, 2003; Shih *et al*, 2003; Figge *et al*, 2004; Gitai *et al*, 2005). Clear evidence for an important role of MreB in cell shape maintenance came from the isolation of spherical *E. coli mreB* mutants more than 20 years ago (Wachi *et al*, 1987), well before the protein was recognized as an actin. About that time the four additional proteins that are currently known to be critical in determining cell shape, MreC, MreD, penicillin-binding protein 2 (PBP2) and RodA were identified as well (Tamaki *et al*, 1980; Wachi *et al*, 1989). The genes for MreC and MreD reside with *mreB* in the *mreBCD* operon, whereas those for PBP2 (MrdA) and RodA (MrdB) reside in the unlinked *mrd* operon. Although MreB is cytoplasmic, MreC and PBP2 are bitopic and MreD and RodA are polytopic cytoplasmic membrane species. PBP2 is the only murein synthase in *E. coli* that is specifically required for extension of the cylindrical portion of the sacculus during cell elongation (Spratt, 1975; de Pedro *et al*, 2001; Vollmer and Bertsche, 2008). RodA is likely needed for proper PBP2 function (Ishino *et al*, 1986; de Pedro *et al*, 2001).

MreC forms a dimer and is thought to interact with MreB, MreD and several of the high molecular weight murein synthases (PBPs), including PBP2 (Divakaruni *et al*, 2005, 2007; Dye *et al*, 2005; Kruse *et al*, 2005; van den Ent *et al*, 2006). MreC, MreD and PBP2 accumulate in a spotty or helical manner along the cell envelope in *E. coli*, *B. subtilis* and/or *C. crescentus* (den Blaauwen *et al*, 2003; Figge *et al*, 2004; Divakaruni *et al*, 2005; Dye *et al*, 2005; Leaver and Errington, 2005). These localization patterns are reminiscent of that of MreB, as well as of the helical patterns of new murein insertion that have been observed along the cylindrical portions of rod-shaped cells. (Daniel and Errington, 2003; Tiyanont *et al*, 2006; Divakaruni *et al*, 2007; Varma *et al*, 2007). Hence, it is proposed that the helical actin fibres function as cytoplasmic tracks for murein synthase and/or hydrolase activities in the periplasm. This would topologically constrain these activities, resulting in helical insertion of new murein and elongation of the cell (Daniel and Errington, 2003; Figge *et al*, 2004; Carballido-Lopez *et al*, 2006).

The MreB cytoskeleton has also been implicated in chromosome segregation in several organisms (Kruse *et al*, 2003, 2006; Soufo and Graumann, 2003; Gitai *et al*, 2005; Srivastava *et al*, 2007). However, such a role is not evident in all bacteria (Hu *et al*, 2007), and additional studies have cast doubt on a critical role of MreB in chromosome segregation in *B. subtilis* and *E. coli* (Formstone and Errington, 2005; Karczmarek *et al*, 2007).

To help elucidate the assembly and/or functions of the MreB cytoskeleton in bacteria, we sought to identify additional proteins required for maintaining the normal rod shape

*Corresponding author. Department of Molecular Biology and Microbiology, School of Medicine, Case Western Reserve University, W213, 10900 Euclid Avenue, Cleveland, OH 44106, USA.
Tel.: +1 216 368 1697; Fax: +1 216 368 3055;
E-mail: pad5@case.edu
[1]Present address: Center for Integrative Genomics, University of Lausanne, Lausanne, Switzerland
[2]Present address: Department of Microbiology and Molecular Genetics, Harvard Medical School, Boston, MA, USA

Received: 8 November 2008; accepted: 24 November 2008; published online: 11 December 2008

of *E. coli* cells. Although *mre* and *mrd* mutants of *E. coli* can propagate as small spheres on poor medium, they succumb to a lethal division defect on rich medium, unless they are supplied with an extra source of the FtsZ cytokinetic protein (Vinella *et al*, 1993; Kruse *et al*, 2005; Bendezu and de Boer, 2008).

We took advantage of this property in a genetic screen for mutants that require extra FtsZ for good growth on rich medium. This led us to identify a well-conserved bitopic membrane protein of unknown function (YfgA) as a new cell shape protein that we named RodZ. Our evidence shows that RodZ is a component of the MreB cytoskeleton, and is required for its normal spiral-like configuration. Analyses of domain deletion/substitution variants identify a juxta-membrane portion of RodZ as essential to its function, and indicate that other domains engage the cell shape machinery in distinct ways. Curiously, although one of these domains resembles a DNA-binding motif, our evidence indicates that it has a dominant function in the association of RodZ with the MreB cytoskeleton.

Results

RodZ (YfgA) is a new cell shape factor in E. coli

In *E. coli*, the five known cell shape maintenance proteins MreBCD and MrdAB are all conditionally essential for growth. Cells lacking any of these proteins propagate stably as small spheres at low mass doubling rates, but form giant non-dividing spheroids at higher ones. An extra supply of the FtsZ division protein, however, suppresses lethality by allowing the shape mutants to propagate as small dividing spheres at higher rates as well (Bendezu and de Boer, 2008). We made use of this latter property in a screen for additional cell shape factors by selecting for transposon mutants that (i) required additional FtsZ for survival or good growth on rich medium and (ii) showed a cell shape defect (see Supplementary data).

Mutant strain Rod2352 was especially interesting as it propagated as spheroids and EZTnkan-2 had inserted in *yfgA*, a gene of unknown function. As mutants both lost rod shape and require an overdose of FtsZ for propagation on LB at or below 30°C (see below), we renamed it *rodZ*. The gene lies immediately upstream of *ispG* (*gcpE*), the product of which catalyses an essential step in isoprenoid biosynthesis (Hecht *et al*, 2001). We next created Δ*rodZ* strains (Figure 1A; Supplementary Table S2). Similar to the original insertion mutant, Δ*rodZ* cells failed to maintain rod shape. The growth properties of Δ*rodZ* cells were complex, and cell shapes depended to some extent on growth conditions. Compared with the wt parent TB28, the mass doubling time of FB60 [Δ*rodZ*] in M9-mal minimal medium increased markedly (from ~64 to >250 min; Tables I and III), but the mutant still formed (small) colonies relatively efficiently on M9 agar (Figure 2A). Cells propagated as spheroids in M9 medium, with few cells displaying more complicated shapes (Figure 2B). Mass doubling time was reduced less in LB medium (~54 versus ~35 min at 37°C; Table I). However, although the mutant still formed colonies on LB agar at 42°C and 37°C, it failed to do so at or below 30°C (Figure 2A, right panels). Cell shapes in LB at these lower temperatures were the most complex, with many cells growing into very large non-dividing spheroids bearing one or more cone-like protrusions (Figure 2B). Comparatively, cell shapes were the least

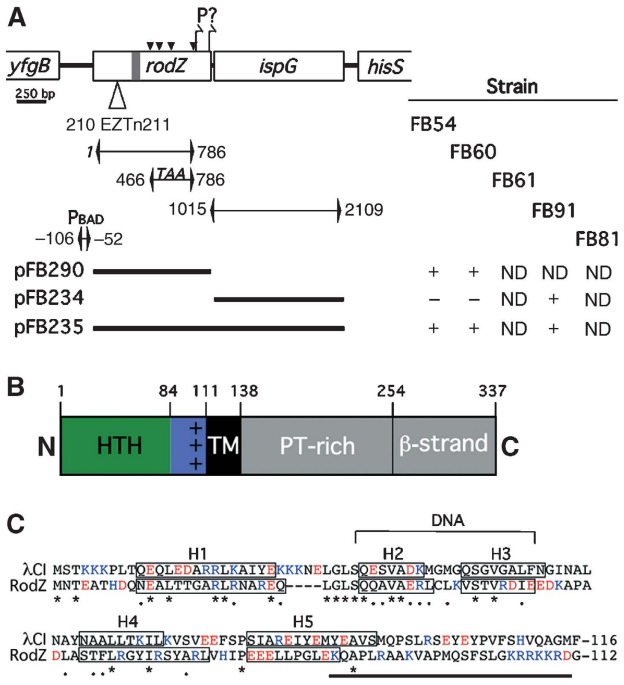

Figure 1 The *E. coli rodZ* locus and predicted RodZ domain structure. (**A**) Insertion sites of the *rod*2352 EZ::Tn transposon (open triangle) and of transposons previously recovered *in rodZ* (Gerdes *et al*, 2003) (black triangles), the positions of chromosomal deletion replacements and corresponding strain designations, inserts in plasmids used for initial complementation assays (thick lines), and the results of these assays. Portions of the chromosome that were replaced with an *aph* cassette, an *frt* scar sequence or a heterologous transcription regulatory cassette (*aph araC* P_{BAD}) are indicated by brackets and adjacent numbers refer to base pairs replaced, counting from the start of *rodZ*. A translation stop (TAA) was placed immediately following codon 155 of *rodZ* in strain FB61. Plasmids carried the indicated inserts downstream of the *lac* regulatory region. +, capable of correcting $RodZ^-$ and/or $IspG^-$ phenotypes; −, incapable of correcting phenotype; ND, not done. (**B**) Predicted domain organization of RodZ. HTH, Cro/CI-type helix-turn-helix motif (green); +++, basic juxta-membrane (JM) domain (purple); TM, transmembrane domain (black); periplasmic (P) domain (grey) with a region rich in prolines and threonines followed by one that may form several β strands. (**C**) Comparison of the cytoplasmic portion of RodZ with the N terminus of λ repressor. Basic residues are in blue and acidic ones in red. Helices 1–5 of λCI, and corresponding predicted helices in RodZ are boxed. Identical (*) and similar (.) residues are indicated. The JM domain (residues 85–111) is underlined.

abnormal on LB at 42°C, although virtually all cells were still misshapen, with many resembling ellipsoids, lemons and/or very wide rods (Figure 2B).

Both the growth and shape defects of Δ*rodZ* cells were fully corrected by pFB290 [P_{lac}::*rodZ*] or other *rodZ* constructs, but not by pFB234 [P_{lac}::*ispG*] (Figure 1; Supplementary Figure S1A; Table I, and see below), showing that neither defect was due to polar effects of the *rodZ* lesion on *ispG* or other genes.

Recovery of the *rodZ*::EZTnkan-2 allele in our screen suggested that moderate overexpression of *ftsZ* is sufficient to suppress lethality of *rodZ* mutants. Accordingly, FB60 [Δ*rodZ*] cells that carried pDR3 [P_{lac}::*ftsZ*] efficiently formed (small) colonies on LB agar at 30°C, provided IPTG was included in the medium (Figure 2C). As with Δ*mre* and Δ*mrd* cells, extra FtsZ allowed Δ*rodZ* cells to propagate as

smaller cells without restoring their shape defects. In M9, this resulted in the formation of smaller spheroids (not shown). In LB, under otherwise non-permissive conditions, extra FtsZ gave rise to heterogeneous populations of severely misshaped cells that frequently displayed branches, bulges and oddly placed and/or angled constrictions (Figure 2D).

We conclude that *rodZ* is critical in maintaining the rod shape of *E. coli*. Similar to the *mreBCD* and *mrdAB* genes (Bendezu and de Boer, 2008), *rodZ* is conditionally essential, and RodZ$^-$ lethality under non-permissive conditions can be suppressed by an elevated level of FtsZ. Additionally, Δ*rodZ* cells displayed a strong medium-dependent growth defect that is not observed in Δ*mre* and Δ*mrd* cells (Bendezu and de Boer, 2008). This defect was not suppressed by elevated levels of FtsZ, by the presence of amino-acid mixtures, or by changing the carbon source (data not shown). Though the reason for this growth phenotype is still unclear, it suggests that RodZ, besides cell shape maintenance, has additional significant function(s) in proliferation.

Table I Growth and shape of *rodZ* cells

Strain[a]	Relevant genotype	IPTG (μM)	T_D[b]	Shape[c]
		LB, 37°C		
TB28	wt	0	35	Rod
FB61	*rodZ*$^{1-155}$	0	37	Rod
FB60	ΔrodZ	0	54	Odd
TB28/pFB290	wt/P_{lac}::*rodZ*	100	38	Rod
FB60/pFB290	Δ*rodZ*/P_{lac}::*rodZ*	100	35	Rod
		M9, 37°C		
TB28	wt	0	64	Rod
FB61	*rodZ*$^{1-155}$	0	68	Rod
FB60	ΔrodZ	0	274	Spheroid
TB28(λFB234)	wt (P_{lac}::*ispG*)	250	62	Rod
FB60(λFB234)	Δ*rodZ* (P_{lac}::*ispG*)	250	298	Spheroid
TB28/pFB290	wt/P_{lac}::*rodZ*	100	92	Rod
FB60/pFB290	Δ*rodZ*/P_{lac}::*rodZ*	100	62	Rod
		M9, 30°C		
TB28(iFB273)	wt (P_{lac}::gfp-rodZ)	250	68	Rod
FB60(iFB273)	ΔrodZ (P_{lac}::gfp-rodZ)	250	68	Rod

[a]Cells were grown at 30°C or 37°C in LB or M9-maltose supplemented with IPTG as indicated.
[b]Mass doubling time in minutes.
[c]Rod, normal rods; spheroid, cells mostly spherical; odd, mixture of bizarre shapes.

RodZ is a conserved, moderately abundant, transmembrane protein with a putative DNA-binding domain

RodZ is a type II (N-in) bitopic membrane protein (Newitt *et al*, 1999) of 337 residues, and is predicted to possess a Cro/CI-type DNA-binding domain near its N terminus (HTH, residues ~1–84). This is followed by a highly basic juxtamembrane region (JM, ~85–110, net charge of +8), a transmembrane domain (TM, ~111–133) and a substantial

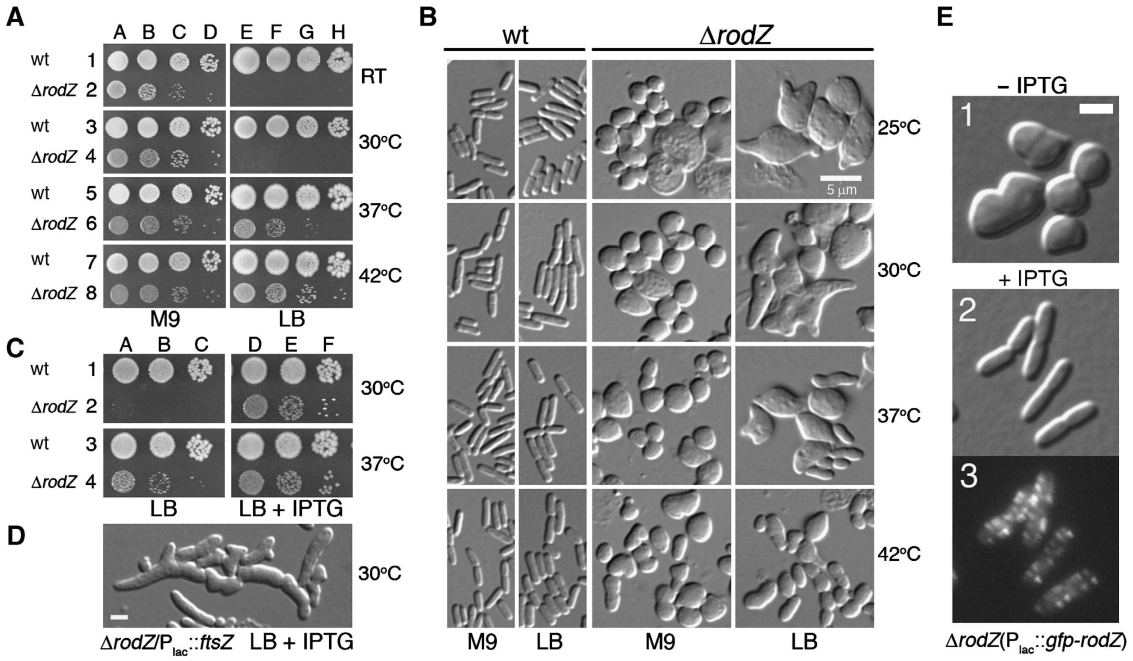

Figure 2 Growth and shape phenotypes of Δ*rodZ* cells, and correction by GFP–RodZ. (**A**) Spot-titre analyses of wt and Δ*rodZ* cells. Strains FB60 [Δ*rodZ*] (uneven rows) and its parent TB28 [wt] (even rows) were grown to density overnight (ON) in M9-mal at 37°C. Cultures were diluted in the same to an optical density at 600 nm (OD_{600}) of 2.4×10^{-2} (columns A and E), 10^{-3} (columns B and F), 10^{-4} (columns C and G) and 10^{-5} (columns D and H), and 10 μl aliquots were spotted on M9-mal (left panel) and LB (right panel) agar. The plates were incubated for 24 (LB) or 48 (M9) h at the indicated temperatures. (**B**) Phenotypes of wt and Δ*rodZ* cells. Aliquots of the ON cultures used in (A) were diluted to $OD_{600} = 0.01$ in M9-mal or LB and grown to $OD_{600} = 0.1$–0.3 at the indicated temperatures. Cells were fixed and imaged by DIC microscopy. (**C**) Suppression of Δ*rodZ*-associated lethality by extra FtsZ. ON cultures of TB28/pDR3 [wt/P_{lac}::*ftsZ*] (even rows) and FB60/pDR3 [Δ*rodZ* / P_{lac}::*ftsZ*] (uneven rows), grown in LB with 50 μM IPTG, were diluted 10^4 (columns A and D), 10^5 (columns B and E) and 10^6 (columns C and F) times in LB, and 10-μl aliquots were spotted on LB plates containing no (columns A–C) or 50 μM (columns D–F) IPTG. (**D**) Phenotype of Δ*rodZ* cells producing extra FtsZ. FB60/pDR3 [Δ*rodZ*/P_{lac}::*ftsZ*] cells were grown at 30°C in LB with 50 μM IPTG to $OD_{600} = 0.3$. Note the branching, bulges and oddly placed constrictions. (**E**) Spiral-like localization of functional GFP–RodZ. FB60(iFB273) [Δ*rodZ* (P_{lac}::*gfp-rodZ*)] cells were grown at 30°C to $OD_{600} = 0.4$–0.5 in M9-mal with no (1) or 250 μM (2,3) IPTG and imaged live with DIC (1,2) or fluorescence (3) optics. Bars equal 5 μm (B) or 2 μm (D, E).

periplasmic domain (P, ~134–337) consisting of a region rich in proline and threonine (~134–253), and a C-terminal domain that may be rich in β-strands (~254–337) (Figure 1B and C). Database searches suggest that RodZ-related membrane proteins with a cytoplasmic Cro/CI (Xre)-type DNA-binding domain are present in many Gram-negative as well as Gram-positive organisms from most bacterial phyla (see COG1426; Tatusov *et al* (2003) and data not shown). The function of none of these has yet been established.

We raised antisera against the purified protein and estimated its cellular abundance by quantitative immunoblotting. The results indicated that RodZ is present at ~650 copies per average exponentially growing cell in LB medium and that its cellular concentration in LB and M9 is about equal (results not shown).

As RodZ resembles a transmembrane transcription factor, we initially considered the possibility that it might be needed for expression of one or more of the other known shape proteins. The compatible plasmids pFB174 [P_{BAD}::*mreBCD*] and pTB59 [P_{lac}::*mrdAB*] can restore rod shape to Δ*mreBCD* and Δ*mrdAB* cells, respectively (Bendezu and de Boer, 2008). However, neither plasmid by itself, or in combination, affected the shape defect of Δ*rodZ* cells, suggesting that this defect was not due to a lack of any of these proteins (Supplementary Figure S1B). In addition, MreB levels in ΔrodZ cells were close to that in wt cells (Supplementary Figure S1C). Together with the finding that the HTH domain is not strictly needed for imposing rod shape *per se* (see below), these observations render it unlikely that RodZ is required for rod shape as a transcription factor.

RodZ localizes in a spiral-type manner along the membrane

Strain FB60(iFB273) [Δ*rodZ*(P_{lac}::*gfp-rodZ*)] expresses GFP–RodZ in an IPTG-dependent manner from a construct (iFB273) that was integrated at the chromosomal *att*HK022 site using the CRIM system (Haldimann and Wanner, 2001). Cells of this strain showed the typical RodZ$^-$ morphology upon growth in medium without inducer (Figure 2E1). However, cell morphology became indistinguishable from wt cells in the presence of IPTG at 250 μM or higher, showing that GFP–RodZ is fully capable of restoring rod shape. Fluorescence microscopy showed a spiral-like distribution of the fusion along the length of cells (Figure 2E3), reminiscent of that previously seen for the MreB cytoskeleton (Kruse *et al*, 2003; Shih *et al*, 2003).

RodZ is part of the spiral-like MreB cytoskeleton

Obtaining a fully functional fluorescent version of *E. coli* MreB by appending fluorescent tags at either terminus proved fruitless (not shown). However, we were able to construct a functional sandwich fusion (MreB–RFP^{SW}) by inserting mCherry RFP between helices 6 and 7 of the protein (van den Ent *et al*, 2001). We then created strains that produce the MreB–RFP^{SW} sandwich under native regulatory control and as the sole actin in the cell. Substitution of *mreB* with *mreB-rfp*^{sw} in these strains was verified by PCR and western blot analyses (Figure 3A and C). Cell morphology and growth rates of *mreB-rfp*^{sw} strains were indistinguishable from wt controls, and MreB–RFP^{SW} was localized in a banded/spiral-like manner along the long axis of cells (Figure 3B and D).

We next co-visualized MreB–RFP^{SW} and GFP–RodZ in cells of strain FB101(iFB273) [*mreB-rfp*^{sw} Δ*rodZ* (P_{lac}::*gfp-rodZ*)] in which production of the former is under native control, that of the latter is IPTG dependent, and the fusions are the sole sources of MreB and RodZ. Cells had a completely normal appearance in the presence of inducer (Figure 3E), implying that both fusions were also functional under these conditions. Notably, the two proteins appeared to colocalize perfectly at all stages of the cell cycle and in all cells examined (Figure 3E, and not shown).

This suggested that the MreB cytoskeleton might function as a scaffold for proper localization of RodZ. As any of the other cell shape proteins may associate with this scaffold as well (Kruse *et al*, 2005), we explored the possibility that they mediate the colocalization of RodZ and MreB. To this end, we co-visualized MreB–RFP^{SW} and GFP–RodZ in strains that completely lack MreC and MreD [Δ*mreCD*], or PBP2 and RodA [Δ*mrdAB*]. These strains also carried pTB63 [*ftsQAZ*], allowing the spherical cells to propagate readily (Bendezu and de Boer, 2008). MreB–RFP^{SW} and GFP–RodZ still colocalized perfectly in either strain, even though the proteins co-accumulated in mostly peripheral clusters/foci rather than in obvious spiral-like patterns (Figure 3F and G). To assess whether such clustering of GFP–RodZ depended on MreB, we examined cells of strain FB30(λFB273)/pTB63 [Δ*mreBCD*(P_{lac}::*gfp-rodZ*)/*fts*QAZ], which lacks all three Mre proteins, as well as in a related strain that lacks MreB specifically. As illustrated in Figure 3H and I, GFP–RodZ distributed evenly along the membrane in spheroids of either strain, showing that MreB indeed directs the cellular location of RodZ.

As their colocalization suggested that RodZ and MreB might interact, we assayed for *in vivo* interactions between RodZ and the other cell shape proteins using the BACTH bacterial two-hybrid system (Table II; Supplementary Figure S2). This system is based on reconstitution of adenylate cyclase activity when the T18 and T25 domains of *Bordetella pertussis* CyaA are brought close together through interactions between fusion partners (Karimova *et al*, 1998).

Each CyaA domain was appended to the cytoplasmic N terminus of RodZ, MreC, MreD, PBP2 or RodA, while it was inserted in between G228 and D229 of MreB to generate MreB–T18^{SW} and MreB–T25^{SW} sandwich fusions. Pairs and inverse pairs of T18 and T25 fusions were co-produced in indicator strain BTH101 [*cya*-99], and putative interactions were assessed by a qualitative plate assay for β-Gal activity (van den Ent *et al*, 2006). Notably, pairing RodZ with MreB produced very strong signals, supporting the notion that the two proteins reside in close proximity *in vivo*. Self-pairing yielded the next strongest signals, suggesting a considerable level of RodZ self-interaction. Interestingly, pairing RodZ with MreC in either genetic configuration also produced clear, but weaker, positive signals. Pairings with MreD or PBP2 yielded even weaker signals at best, and pairings with RodA yielded essentially no signals above those obtained with unfused T18 or T25 controls (Table 2; Supplementary Figure S2).

We conclude that RodZ is an integral component of the MreB cytoskeleton.

Aberrant assembly of MreB in RodZ$^-$ cells

To assess how RodZ affects MreB localization, we first examined the distribution of MreB–RFP^{SW} in spheroids of

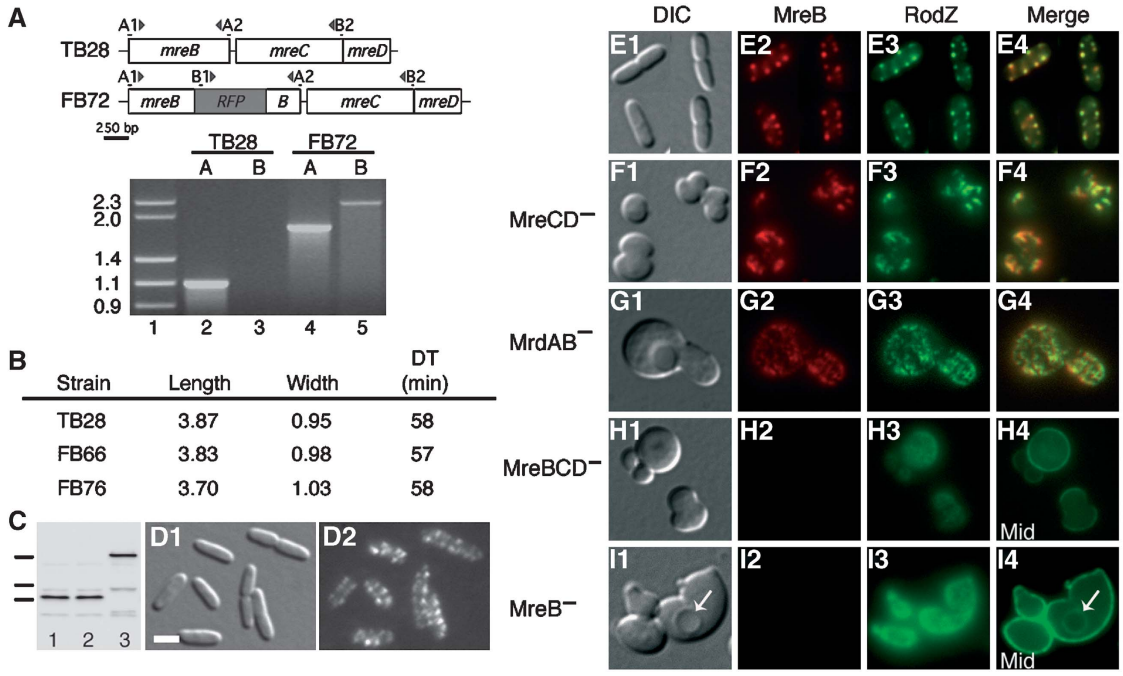

Figure 3 Construction of a functional MreB–RFP^{SW} sandwich fusion, and colocalization of MreB and RodZ. (**A–D**) Construction and analyses of a chromosomally encoded MreB–RFP^{SW} sandwich fusion. (A) The *mre* loci of wt and *mreB-rfp*^{SW} strains, illustrating the location of the *rfp* ORF within that of *mreB* in strain FB72 and its derivatives, is shown. The annealing sites and orientations of primers A1 and A2 (pair A) and B1 and B2 (pair B) are indicated. These pairs were used to amplify chromosomal DNA of TB28 [wt] (lanes 2 and 3) or FB72/pCX16 [*mreB-rfp*^{SW}/*sdiA*] (lanes 4 and 5) by PCR, and the products were analysed by agarose gel electrophoresis. Size standards (in kb) are shown in lane 1. For (B, C), ON cultures of TB28 [wt], FB66 [*yhdE*<>*cat*] and FB76 [*mreB-rfp*^{SW} *yhdE*<>*cat*] were diluted in LB to $OD_{600} = 0.01$ and grown at 30°C. Mass doubling rates were determined by measuring OD_{600} at 1-h intervals. At $OD_{600} = 0.5$, aliquots were used for the determination of cell shape parameters or for the preparation of whole-cell extracts. Note that *yhdE*<>*cat* was used as a selectable marker for transduction of the closely linked *mreB-rfp*^{SW} allele into various strain backgrounds. (B) The cell doubling times and the average cell length and width ($n = 200$) of the three strains are listed. (C) A western blot of the corresponding extracts from strains TB28 (lane 1), FB66 (2) and FB76 (3) is shown. Each lane received 10 μg total protein, and MreB (37.0 kDa, lanes 1 and 2) and MreB–RFP^{SW} (64.3 kDa, lane 3) were detected by using affinity-purified α-MreB antibodies. The positions of 66, 45 and 36 kDa standards are indicated. (D) DIC (D1) and fluorescence (D2) images of FB83 [*mreB-rfp*^{SW} *yhdE*<>*frt*] cells that were grown to $OD_{600} = 0.5$ in M9-mal are shown. Note the normal rod shape of cells, and the spiral-like distribution of MreB–RFP^{SW}. (**E–G**) Colocalization of MreB and RodZ. Corresponding DIC (1), RFP (2), GFP (3) and merged fluorescence (4) images are shown. (E) The colocalization of MreB–RFP^{SW} and GFP–RodZ in rod-shaped cells in which these functional fusions are the only MreB and RodZ proteins present are shown. Note the perfect colocalization in the typical spiral-like cytoskeleton. (F, G) Mreb–RFP^{SW} and GFP–RodZ still colocalize in more disorganized patterns at the periphery of spheroids that are completely devoid of MreC and MreD (F), or of MrdA (PBP2) and MrdB (RodA) (G). The focal plane was near the top of cells in (F, G). (**H**, **I**) Location of RodZ in the absence of MreB. Corresponding DIC (1), RFP (2) and GFP (3 and 4) fluorescent images are shown. The panels show the distribution of GFP–RodZ in spheroids that either lack all three Mre proteins (H) or MreB specifically (I). The focal plane was near the top (panels 3) or through the interior (panels 4) of the spheroids. Note the even distribution of GFP–RodZ along the cell membrane, including along that of an intra-cytoplasmic vesicle visible in (I) (arrow). Strains used for (E–I) were: FB101(iFB273) [*mreB-rfp*^{SW} Δ*rodZ* (P_{lac}::*gfp-rodZ*)] (E), FB95(iFB273)/pTB63 [*mreB-rfp*^{SW} Δ*mreCD*(P_{lac}::*gfp-rodZ*)/*ftsQAZ*] (F), FB90(iFB273)/pTB63 [*mreB-rfp*^{SW} Δ*mrdAB*(P_{lac}::*gfp-rodZ*)/*ftsQAZ*] (G), FB30(λFB237)/pTB63 [Δ*mreBCD*(P_{lac}::*gfp-rodZ*)/*ftsQAZ*] (H) and FB30(λFB237)/pTB63/pFB206 [Δ*mreBCD* (P_{lac}::*gfp-rodZ*)/*ftsQAZ* /P_{BAD}::*mreCD*] (I). Cells were grown ON in M9-mal with 250 μM IPTG and either no (E–H) or 0.05% (I) arabinose. After dilution to $OD_{600} = 0.1$ in the same medium, growth was continued to $OD_{600} = 0.4–0.6$, and cells were imaged live. Note that under the same conditions, pFB206 directs the production of sufficient MreC and MreD to correct the shape defect of a Δ*mreCD* strain (not shown). Bar equals 2 μm.

strain FB85/pTB63 [*mreB-rfp*^{SW}Δ*rodZ* /*ftsQAZ*], that lack RodZ entirely. As noted above, MreB–RFP^{SW} accumulated in numerous small patches/foci of comparable intensity along the membrane of spheroids that are devoid of MreCD or MrdAB (Figures 3F, G and 4A). In comparison, MreB–RFP^{SW} concentrated in notably fewer and larger peripheral clusters in RodZ^{-} spheroids. This was especially apparent in LB-grown Δ*rodZ* spheroids, in which most of MreB–RFP^{SW} accumulated in a small number (~1–4) of intensely stained clusters (Figure 4B and C).

To explore whether this aberrant assembly of MreB is more likely a cause or a consequence of the loss of cell shape in Δ*rodZ* cells, we monitored MreB–RFP^{SW} during depletion of RodZ from cells of strain FB81 [*mreB-rfp*^{SW}P_{BAD}::*rodZ*] in which chromosomal *rodZ* is under control of the *ara* regulatory region. Although virtually all cells were still rod-shaped after growth in the absence of arabinose for 3.3 mass doublings, about half of them already displayed a small number of intense MreB–RFP^{SW} accumulations, and the typical spiral-like distribution of the protein was not or poorly discernible in these cells (Figure 4E). Even after an additional 2.3 doublings, cells were still rod-shaped (though wider than normal), but the majority now displayed intense and aberrant MreB–RFP^{SW} assemblies (Figure 4F).

These results indicate that RodZ has an important function in the formation of the extended spiral-like configuration of the MreB cytoskeleton typically seen in rod-shaped cells. Furthermore, as aberrant assembly of MreB precedes the loss of cell shape during depletion of RodZ it is likely that the shape phenotype of RodZ^{-} cells is, at least

Table II RodZ interactions detected by bacterial two-hybrid assays

T18–[a]	RodZ aa missing	T25–[b]						
		U[c]	RodZ	MreB	MreC	MreD	PBP2	RodA
RodZ	None	–	+ + +	+ + + +	+ +	+	+	–
ΔHTH	1–82	–	+	+ +	+	–	–	–
HTH-M	85–337	–	+ +	+ + + +	–	–	–	–
ΔJM	85–110	–	+ + +	+ + + +	+ +	+	+	–
					T18–[b]			
		U	RodZ	MreB	MreC	MreD	PBP2	RodA
T25–RodZ[a]	None	–	+ + +	+ + + +	+ +	–	–	–

[a]CyaA domain appended to N terminus of full-length RodZ$^{1-337}$ (RodZ); RodZ$^{83-337}$ (ΔHTH); RodZ$^{1-84}$–MalF$^{1-39}$–RFP (HTH-M) or RodZ$^{1-84}$–MalF$^{1-16}$–RodZ$^{111-337}$ (ΔJM).
[b]CyaA domain unappended (U) or appended to N terminus of full-length protein, except for MreB wherein the domain was inserted to create a sandwich fusion (see text).
[c]Qualitative measure of β-galactosidase production. Colonies of strain BTH101 [*cya*-99] carrying appropriate plasmid pairs were patched on indicator plates and inspected for colour development after 24, 30 and 36 h. –, white at 36 h; +, white at 24 h, but light colouring afterwards; + +, light colouring at 24 h and medium blue afterwards; + + +, medium blue at 24 h and dark blue afterwards; + + + +, dark blue at 24 h and afterwards.

partly, caused by the inability of MreB to form a proper cytoskeleton.

Rod shape depends on a proper MreB to RodZ ratio

Overexpression of MreB was previously reported to cause a cell division defect (Wachi and Matsuhashi, 1989; Kruse *et al*, 2003). We noticed, however, that the effects of MreB or RodZ overexpression in either TB28 [wt] (not shown) or FB83 [*mreB-rfp*^{sw}] (Figure 5) cells depend strongly on the growth medium. When cells harbouring pFB216 [P_{tac}::*mreB*] were grown in LB with IPTG (250 μM), they became filamentous, as expected, though the filaments were also notably wider than wt rods (average diameter $D = 1.7$ μm versus $D = 1.0$ μm; see Supplementary Table S1). In contrast, when MreB was overexpressed in M9 medium (~2.5-fold; Figure 5F), cells lost shape and formed large non-dividing spheroids (Figure 5C). Similarly, overexpression of RodZ from the compatible plasmid pFB291[P_{tac}::*rodZ*] caused some elongation and widening of cells in LB (Supplementary Table S1), but overexpression in M9 (~6.5-fold; Figure 5F) led to a complete loss of rod shape. In such M9-grown spheroids of strain FB83/pFB291 [*mreB-rfp*^{sw}/P_{tac}::*rodZ*], MreB–RFP^{SW} accumulated in large clusters (Figure 5B), indicating that both the lack (Figure 4B–F) and overabundance of RodZ can cause MreB to form large structures that are ineffective in directing proper cell elongation.

Interestingly, co-overexpression of MreB and RodZ in FB83/pFB216/pFB291 prevented the loss of cell shape seen when either protein is overexpressed alone. Instead, cells formed long and narrow ($D = 0.8$–0.9 μm; Supplementary Table S1) filaments in either medium (Figure 5D). Thus, maintenance of a cylindrical cell shape depends critically on a proper MreB to RodZ ratio. In addition, it appears that MreB and RodZ significantly reinforce each other's ability to inhibit cell division when present at elevated levels.

Unique nucleoid and MreB/RodZ distribution patterns upon co-overexpression of MreB and RodZ

In addition to the division defect, cells that co-overexpressed RodZ and MreB showed other notable features. First, filaments of either TB28 [wt] (not shown) or FB83 [*mreB-rfp*^{sw}] showed unusually large nucleoid-free gaps, suggesting a defect in chromosome integrity, replication or segregation (Figure 5D3 and E3). Second, inspection of MreB–RFP^{SW} spirals in such filaments of strain FB83 revealed that they were not evenly distributed along the long axis of the filaments, but became enriched in zones that almost always corresponded to a nucleoid-free gap (Figure 5D2 and E4, arrowheads). Third, over a third (39/105) of the filaments showed one or two prominent bulges, and these were always enriched with MreB–RFP^{SW}. Curiously, all such bulges also contained DAPI-stained material, and often a substantial amount, as if these were sites where nucleoids had invaded an MreB-enriched zone, or vice versa (Figure 5D, arrow).

We expected RodZ to co-enrich with MreB under these conditions as well. To verify this, we imaged cells of strain FB83/pFB299/pFB309 [*mreB-rfp*^{sw}/P_{tac}::*mreB rodZ*/P_{syn35}::*gfp-rodZ*], in which MreB and RodZ can be overexpressed from a single plasmid, and production of GFP–RodZ is under control of a weak constitutive promotor on a compatible plasmid. Figure 5E shows an example of filaments of this strain after growth in the presence of IPTG, and when they are still relatively short. Note that they still contain an even number of fairly well separated (pairs of) nucleoids, suggesting that chromosome replication had proceeded apace. However, nucleoids failed to distribute normally towards the poles of the filaments, leaving large nucleoid-free zones at each cell end, and these were also the regions where GFP–RodZ had indeed preferentially co-accumulated with MreB–RFP^{SW}. Moreover, filament ends at which an MreB/RodZ-enriched zone substantially overlapped the nearest nucleoid, often already showed some local widening of the cell cylinder (Figure 5E, arrows). On further growth, filaments of this strain showed phenotypes as that described for FB83/pFB216/pFB291 (Figure 5D), with both proteins enriched at both internal and polar nucleoid-free zones, as well as at more pronounced bulges (not shown).

Depletion of RodZ does not greatly affect chromosome segregation

The MreB cytoskeleton has been implicated in chromosome segregation (Kruse *et al*, 2003, 2006; Soufo and Graumann, 2003; Gitai *et al*, 2005). Given its properties described above, RodZ would be an attractive candidate for mediating MreB-directed nucleoid dynamics. However, inspection of DAPI-treated FB60 [ΔrodZ] cells failed to reveal DNA-less cells (0/200) or any other gross nucleoid segregation defects

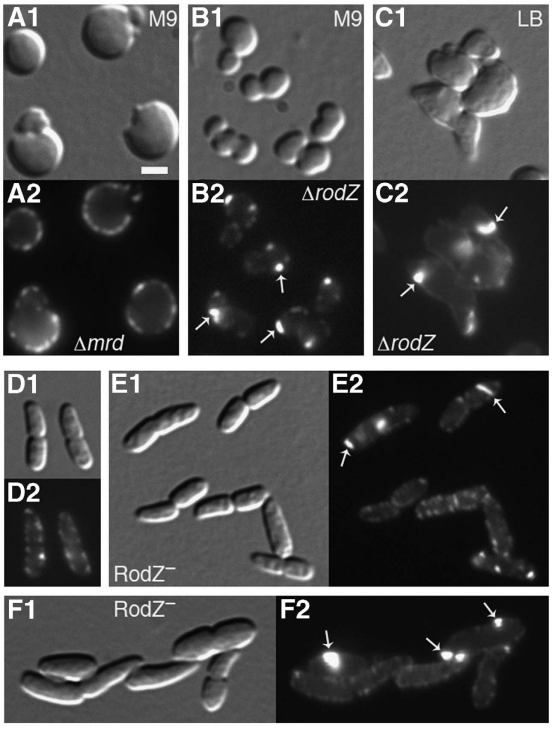

Figure 4 RodZ-dependent localization of MreB. (**A–F**) Formation of large aberrant MreB patches in RodZ$^-$ cells. Corresponding DIC (panels 1) and RFP fluorescence (panels 2) images of live cells are shown. Localization of MreB–RFP^{SW} in Δ*mrdAB* (A) or Δ*rodZ* (B, C) spheroids. Note the numerous small fluorescent spots along the periphery of Δ*mrdAB* cells versus the less numerous and larger patches of MreB–RFP^{SW} that accumulate at the periphery of Δ*rodZ* cells (arrows) in either minimal (B) or rich (C) medium. Strains used were FB90/pTB63 [*mreB-rfp*^{SW} Δ*mrdAB/ftsQAZ*] (A), and FB85/pTB63 [*mreB-rfp*^{SW} Δ*rodZ/ftsQAZ*] (B, C). ON cultures in M9-mal were diluted to $OD_{600} = 0.1$ in the same (A, B) or in LB (C) and growth was continued to $OD_{600} = 0.4–0.5$. (D–F) Depletion of RodZ leads to the formation of such MreB patches well before cells become grossly misshapen. The RodZ-depletion strain FB81 [*mreB-rfp*^{SW} P_{BAD}::*rodZ*] was grown ON in M9-mal with 0.5% arabinose, diluted to $OD_{600} = 0.05$ (D, E) or $OD_{600} = 0.01$ (F) in LB with 0.5% (D) or no (E, F) arabinose, and growth was continued to $OD_{600} = 0.4–0.5$. Bar equals 2 μm.

(Supplementary Figure S3D and E). Moreover, we failed to detect any obvious defects in segregation of the origin and terminus regions of the chromosome during depletion of RodZ (Supplementary Figure S3). These results indicate that a lack of RodZ has little, if any, direct effect on chromosome dynamics.

Roles of RodZ domains in cell growth, cell shape and RodZ localization

In genetic footprinting analyses of the *E. coli* genome, *rodZ* (*yfgA*) was classified as non-essential because a transposon insertion in codon 156 was apparently well tolerated by cells growing in rich medium (Gerdes *et al*, 2003). This prompted us to engineer a strain bearing a translation stop after codon 155 of chromosomal *rodZ* (Figure 1A). Indeed, FB61[*rodZ*$^{1-155}$] cells grew well and were still rod-shaped in both minimal and rich medium, though they were up to 45% wider on average than cells of the wt parent TB28 (Table I; Supplementary Figure S4). Thus, the periplasmic part of RodZ is largely dispensable, although it may help to fine-tune the precise dimensions of cells.

We next studied the roles of each of the HTH, basic JM, TM and P domains in RodZ function. To this end, we created a set of derivatives of the integrative CRIM construct pFB273 [P_{lac}::*gfp-rodZ*], encoding variants of GFP–RodZ in which one or more of the domains is missing or replaced. To replace the JM and/or TM domain, we used corresponding domains of MalF (TM1; Guzman *et al*, 1997), and mCherry replaced the P domain in some variants.TB28 [wt] and FB60 [Δ*rodZ*] cells producing each variant were then examined for growth rate, cell morphology and localization of the mutant protein (Figure 6; Table 3). Western blot analyses indicated that none of the variants was subject to excessive degradation (Supplementary Figure S5).

Notably, the results in toto (Figure 6; Table III) revealed that both normal growth rate and cell shape is strictly dependent on: (i) the JM domain of RodZ (Figure 6, compare A with I, D with E and F with G), (ii) a TM domain to anchor it to the membrane (Figure 6, compare B and D with C), and (iii) the JM–TM part of RodZ being either preceded by its HTH domain, or followed by its P domain (Figure 6, compare B and F with H). Furthermore, although substitution of RodZ's TM with TM1 of MalF did not abolish RodZ function, the comparable variant with RodZ's native TM was clearly more effective in restoring rod shape to Δ*rodZ* cells (Figure 6B and D; Table III).

Surprisingly, the requirements for a normal localization pattern of RodZ were not the same as those for good growth and rod shape of cells. Thus, a membrane-tethered version of the HTH domain was both required (Figure 6C and F–H) and sufficient (Figure 6B, D, E and I) for the protein to sharply accumulate spiral-like in rods or in peripheral foci in non-rods.

The properties of a fusion lacking the HTH domain (GFP–RodZ$^{83-337}$) were particularly revealing as it still restored rod shape to a majority of Δ*rodZ* cells, even though many rods appeared wider than normal and the rest of the population (~25%) showed irregularities such as uneven width, branching and/or a spheroidal shape (Figure 6F; Table III). However, the protein distributed far more evenly along the membrane in both corrected Δ*rodZ* rods and wt cells (Figure 6F) than HTH+ variants (Figure 6A, B, D, E and I). The distribution of GFP–RodZ$^{83-337}$ was not completely homogeneous, however, suggesting that some of the protein still accumulated in a more organized manner (Figure 6F3 and F4).

These results showed that the HTH domain is not strictly required for RodZ function *per se*, but that it is responsible for the typically sharp spiral-like distribution of the protein. In turn, this indicated that the HTH domain contributes significantly to the association of RodZ with the MreB cytoskeleton, and this was supported by BACTH assays. A membrane-tethered fusion containing just the HTH domain (T18–RodZ$^{1-84}$–MalF$^{1-39}$–RFP) still showed a very strong interaction with MreB (T25–MreB^{SW}) as well as a weaker one with full-length RodZ (T25–RodZ). In contrast, interactions with MreC or the other shape proteins were no longer obvious with this fusion, suggesting that these require other parts of RodZ (Table II; Supplementary Figure S2). Conversely, a fusion lacking just the HTH domain (T18–RodZ$^{83-337}$) still showed interactions with MreB, RodZ, as well as MreC, but all three appeared distinctly weaker than those seen with

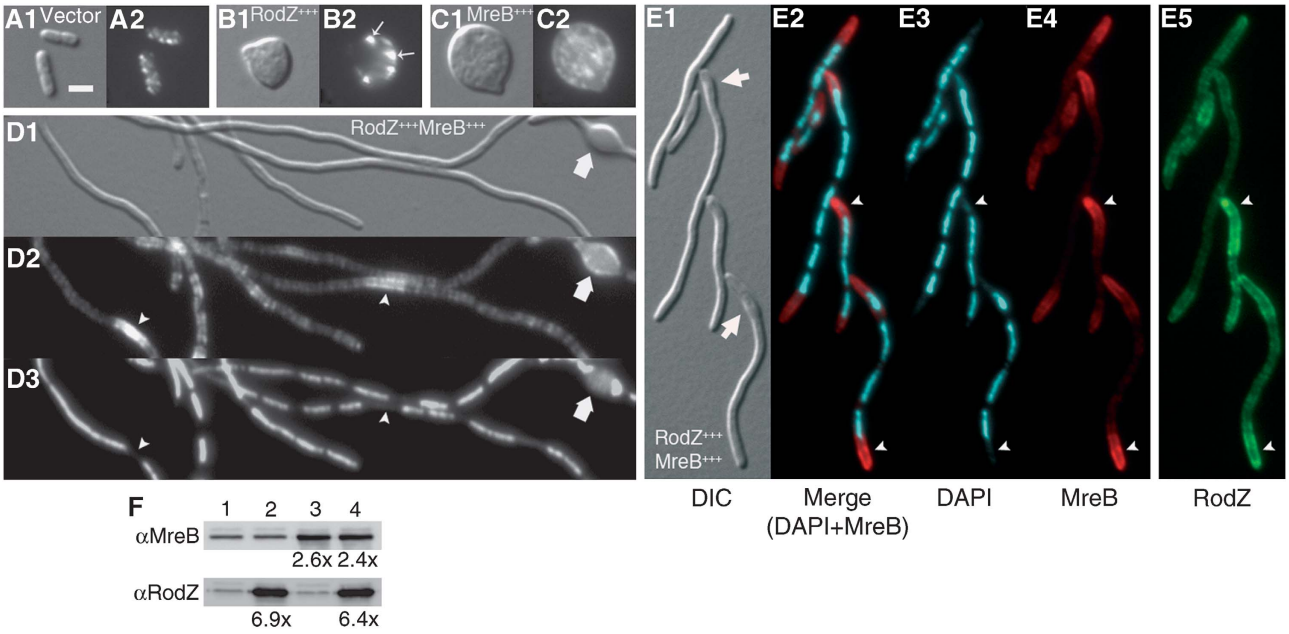

Figure 5 The RodZ to MreB ratio is important for rod shape maintenance. (**A–D**) illustrate the effects of overproduction of RodZ (B), MreB (C) or both (D) on cell shape in minimal medium. Arrow heads in (D) point at MreB-enriched zones that form at nucleoid-free gaps in the filaments, and the arrow points at a prominent bulge. Cells of strain FB83 [*mreB-rfp*^{sw}] harbouring vector pJF188EH [vector] (A), pFB291 [P_{tac}::*rodZ*] (B), pFB216 [P_{tac}::*mreB*] (C) or both pFB291 and pFB216 (D), were inoculated to $OD_{600} = 0.005$ in M9-mal with appropriate antibiotics and 100 (B) or 250 (A, C, D) μM IPTG. After growth to $OD_{600} = 0.5$, cells were fixed and imaged with DIC (1), RPF (2) or DAPI (D3) optics. Identical effects on cell morphology were seen with TB28 [wt] as host (not shown). (**E**) Co-enrichment of MreB–RFP^{SW} and GFP–RodZ at large nucleoid-free gaps (arrowheads) at the ends of filaments co-overproducing RodZ and MreB. Cells of strain FB83/pFB299/pFB309 [*mreB-rfp*^{sw} /P_{tac}::*mreB*::*rodZ*/P_{syn135}::*gfp-rodZ*] were grown in M9-mal with 250 μM IPTG to $OD_{600} = 0.5$, fixed and treated with DAPI. DIC (1), DAPI + RFP merged (2), DAPI (3), RFP (4) and GFP (5) fluorescence images are shown. Arrows in panel 1 point at areas of local widening of the cell cylinder at sites where the enrichment zone of the two shape proteins overlaps an adjacent nucleoid. (**F**) Overexpression levels of RodZ and MreB. TB28 [wt] cells containing the plasmid pairs pJF188EH [vector] and pBAD33 [vector] (1), pFB291 [P_{tac}::*rodZ*] and pBAD33 (2), pJF118EH and pFB216 [P_{tac}::*mreB*] (3) or pFB291 and pFB216 (4) were grown as described for (A–D) and prepared for quantitative western blot analyses. Each lane received 10 μg total protein and MreB (upper) and RodZ (lower) were detected with specific antisera. Levels relative to wt (lane 1) are given under the relevant lanes. The effects of RodZ and/or MreB overexpression on cell morphology were identical to that shown for FB83 in A–D. Bar equals 2 μm.

the full-length T18–RodZ fusion (Table II; Supplementary Figure S2).

As the JM domain of RodZ is essential for its function in cell shape maintenance, we also explored whether its substitution affected its interactions with cell shape proteins in the BACTH assay. However, the interaction pattern of a T18–$RodZ^{1-84}$–$MalF^{1-16}$–$RodZ^{111-337}$ fusion was very similar to that of T18–RodZ (Table II; Supplementary Figure S2). This suggests that, if any interaction between the JM domain and other shape proteins occurs, these may be relatively weak and/or short-lived compared with those involving other domains of RodZ.

Discussion

A novel genetic screen for cell shape mutants of *E. coli* led us to uncover RodZ as a new cell shape factor in bacteria. Like the MreBCD and MrdAB proteins, RodZ has a critical function in the maintenance of rod shape and is conditionally essential for viability. Though *rodZ* (*yfgA*) had no known function, we note that the ill-defined *divD* lesions of classical round-cell mutants of *Salmonella typhimurium* mapped very near the location of *rodZ* (Wyche *et al*, 1974), suggesting that these may have been allelic.

The phenotypes of Δ*rodZ* cells showed similarities as well as interesting differences with *mre* and *mrd* shape mutants (Bendezu and de Boer, 2008). Similar to the latter, Δ*rodZ* cells showed division defects and could grow into giant spheroids with elaborate intra-cytoplasmic membrane systems (e.g. Figure 6C, G and H). In addition, Δ*rodZ* cells showed conditional lethality on rich medium, which was suppressible by extra FtsZ (Figure 2). Unlike *mre* and *mrd* mutants, however, lethality on rich medium of Δ*rodZ* cells was also partially suppressed by growth at 42°C, and cell shape appeared the least abnormal then as well. This suggests that some other factor can partially compensate for the lack of RodZ under these conditions. It is unclear what this factor might be, but it is unlikely to be any of the other cell shape proteins (Supplementary Figure S1). Furthermore, although *mre*- and *mrd*-null mutants form spheroids exclusively, Δ*rodZ* cells often displayed more complex shapes, especially under non-permissive conditions (LB, <37°C). This might be a direct consequence of the misassembly of MreB into the large clusters seen in these cells. If such non-spiral assemblies still were to direct some new murein synthesis, it is easy to imagine this leading to bizarre cell shapes.

Another notable difference with *mre* and *mrd* mutants is the large reduction of mass doubling rates of Δ*rodZ* versus wt cells in M9 medium. This growth defect likely helps Δ*rodZ* cells to survive on this medium, as forced reduction of growth rates helps *mre* and *mrd* mutants to survive as well (Bendezu and de Boer, 2008). Our mutational analyses so far

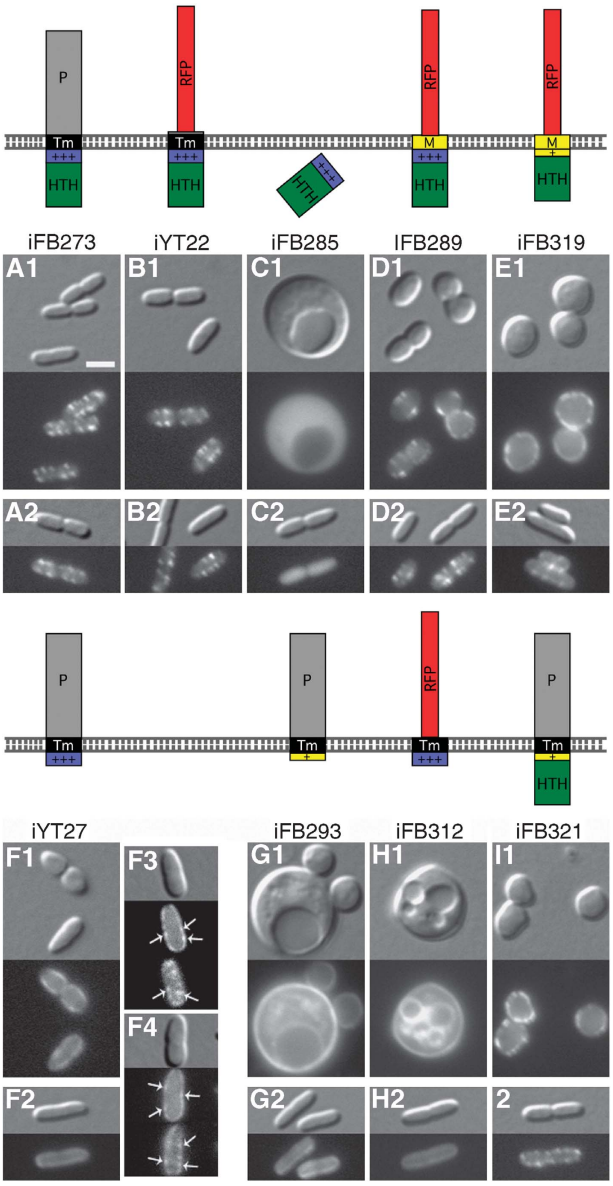

Figure 6 Domains required for normal RodZ localization and cell shape. (**A–I**) FB60 [ΔrodZ] (1) and TB28 [wt] (2) cells expressing various GFP-tagged mutant variants of RodZ from a construct integrated at the chromosomal *att*HK022 site. Construct names are indicated above the panels. The domain architecture of each RodZ variant is depicted above the corresponding cell images: HTH (helix-turn-helix, green); + + + (=JM, juxta-membrane, purple); TM (transmembrane, black); P (periplasmic, grey); + ($MalF^{1-14}$, yellow); M ($MalF^{17-39}$, yellow); RFP (mCherry, red). Each variant contained GFP at its N terminus (not indicated). Cells were grown ON at 30°C in M9-mal with 250 μM IPTG, and diluted to $OD_{600}=0.05$ in fresh medium. Growth was continued to $OD_{600}=0.3$–0.5, and cells were imaged live with DIC and GFP fluorescence optics. (F3, F4) show the presence of faint foci (arrows) within the peripheral haze formed by GFP–$RodZ^{83-337}$ (ΔHTH-RodZ) in two cells of strain FB60(iYT27), imaged with focus through the middle (middle image) or near the top (lower image) of the cells. Bar equals 2 μm.

failed to separate the roles of RodZ in growth and cell shape (Table III). Further work may do so, or a single RodZ activity may control both cell shape and growth rate. It will be interesting to learn the precise cause of this growth defect, as it suggests that RodZ links the cell shape machinery with some cellular activity that is especially important for cell proliferation on poor medium.

Apart from the cell shape phenotypes of Δ*rodZ* cells, our conclusion that RodZ is a component of the MreB cytoskeleton is supported by the colocalization of RodZ and MreB (Figures 3 and 5), by BACTH assays indicating that RodZ interacts with MreB and MreC *in vivo* (Table II; Supplementary Figure S2), and by evidence that the ratio of MreB to RodZ must be kept within limits to ensure an elongated cell shape (Figure 5).

Furthermore, the atypical accumulation of MreB in dense clusters in cells lacking RodZ (Figure 4) implies that the protein has a critical function in ensuring assembly of the cytoskeleton into its typical spiral-like configuration. In eukaryotes, the dynamics and architecture of F-actin are modulated by a plethora of actin-binding proteins that function at a variety of steps in assembly/disassembly reactions (Pollard, 2007). RodZ may similarly modulate MreB assembly directly. Robust *in vitro* systems will be needed to address whether it does so and, if so, at what step(s).

Our domain analyses (Figure 6; Table III) show that the basic juxta-membrane (JM) domain of RodZ is the only one that is strictly required for the maintenance of rod shape. Hence, this domain is likely the most directly involved in ensuring a proper configuration of the MreB cytoskeleton. The JM domain is clearly not sufficient for RodZ function, however, as the domain also needs to be membrane-tethered and, additionally, needs to be accompanied by either the cytoplasmic HTH or the periplasmic P domain (Figure 6; Table III). These results are inconsistent with a simple binary interaction between RodZ and the cytoskeleton, but rather argue that RodZ engages cytoskeletal partners on both sides of the membrane.

The most parsimonious scenario that is consistent with all our data has the following features: (i) the JM domain of RodZ directly or indirectly coaxes MreB fibres into a spiral-like configuration, ensuring that cells establish/maintain a proper long axis. (ii) The JM domain itself has insufficient affinity for the cytoskeleton to stably associate with it. (iii) The HTH and P domains each contribute separately, and to different extents, to the association of RodZ with the cytoskeletal apparatus. This ensures that, even when one of these domains is missing, the local concentration of JM domains near MreB fibres in the cytoplasm remains sufficiently high to stimulate rod shape in a majority of cells. (iv) The HTH domain is the dominant localization determinant of RodZ, and directly or indirectly engages MreB in the cytoplasm (Figure 6; Tables II and III). As RodZ and MreB still colocalized sharply in the absence of the other cell shape proteins (Figure 3), it is unlikely that they mediate this interaction. The simplest interpretation is that the HTH domain binds MreB directly, but this needs to be confirmed with purified components. (v) In the periplasm, the P domain engages another transmembrane component of the cell shape machinery that itself associates with the MreB cytoskeleton. In rod-shaped cells producing only the ΔHTH variant of RodZ, some of the protein could still be detected in weak spots or bands, but it localized far less sharply than HTH^+ variants and was clearly less effective in imposing rod shape than the ΔP variant (Figure 6; Table III). This suggests that the P domain alone is only moderately effective in keeping RodZ incorporated into the cytoskeleton. What the P domain partners with remains to be established firmly, but MreC is an attractive candidate as

Table III Phenotypes of RodZ deletion/substitution derivatives

Integrated construct	Fusion: GFP–	Domain(s) missing or substituted[a]	FB60 [Δ*rodZ*][b]				TB28 [wt][b]
			T_D (min)[c]	% rod-like[d,e]	Other shapes[d,f]	Loc[d,g]	Loc[d,g]
iFB273	$RodZ^{1-337}$	None	68	>99	None	Sp	Sp
iYT22	$RodZ^{1-138}$–RFP	P	86	>99	None	Sp	Sp
iFB285	$RodZ^{1-111}$	TM + P	518	<1	Spheroid	C	C
iFB289	$RodZ^{1-111}$–$MalF^{17-39}$–RFP	TM + P	82	45	Mix	Sp	Sp
iFB319	$RodZ^{1-84}$–$MalF^{1-39}$–RFP	JM + TM + P	301	<1	Spheroid	Sp	Sp
iYT27	$RodZ^{83-337}$	HTH	76	76	Mix	M + Sp	M + Sp
iFB293	$MalF^{2-14}$-$RodZ^{111-337}$	HTH + JM	401	<1	Spheroid	M	M
iFB312	$RodZ^{83-138}$–RFP	HTH + P	602	<1	Spheroid	M	M
iFB321	$RodZ^{1-84}$–$MalF^{1-14}$–$RodZ^{111-337}$	JM	245	4	Mix	Sp	Sp

[a]HTH, helix-turn-helix-like; JM, basic juxta-membrane; TM, transmembrane; P, periplasmic.
[b]Cells were grown as described in the legend of Figure 6.
[c]Mass (OD_{600}) doubling time.
[d]Between 50 and 300 cells were observed in detail in each case.
[e]Cells with distinct short and long axes that resembled a capsule rather than a lemon.
[f]Spheroid, >90% of cells were spheroids of different sizes; mix, cells resembled spheroids; lemons, appeared branched, or had other atypical shapes.
[g]Localization pattern of RodZ variant. Sp, spiral-like and/or spotty along membrane; C, throughout cytoplasm; M, evenly along membrane.

BACTH assays now suggest that MreC interacts with MreB and MreD (Kruse *et al*, 2005; our unpublished results), as well as with RodZ (Table II; Supplementary Figure S2).

Though the primary structure of the HTH domain suggests a DNA-binding function, depletion of RodZ had little, if any, effect on nucleoid segregation (Supplementary Figure S3). In addition, our evidence strongly indicates that the domain is actually used to engage the cytoskeleton. Still, interactions between RodZ and the chromosome remain possible. The unique inverse distribution patterns of nucleoids and MreB/RodZ-enriched zones in filaments that co-overexpress the proteins suggest that nucleoids somehow determine the positioning of these zones or vice versa (Figure 5). In turn, this suggests the possibility that cytoskeletal function may somehow be modulated by the underlying nucleoid. This will require further investigation, as will a full understanding of other aspects of the complex phenotype caused by increased levels of MreB and RodZ.

Very recently, we learned (personal communication) that two other groups independently identified RodZ as an important cell shape factor in *E. coli* (Shiomi *et al*, 2008) as well as in *C. crescentus* (Christine Jacobs-Wagner). The latter emphasizes the likelihood that RodZ function has been widely conserved among the bacteria.

In addition to the discovery and initial characterization of RodZ, we also described the creation of a functional MreB–RFP^{SW} sandwich fusion, which we exploited throughout this study and should prove useful in future studies on the cytoskeleton. Evidently, the presence of an extra domain between helices 6 and 7 can be remarkably well tolerated by *E. coli* MreB. It will be worth exploring if this is true for other (bacterial) actins as well.

Materials and methods

E. coli strains, plasmids, phages, growth conditions, BACTH assays and rod *screen*

Details on all strains (Supplementary Table S2), genetic constructs (Supplementary Table S3) and their source or construction are provided as Supplementary data. Relevant genotypes [in brackets] are also given in the text.

Unless stated otherwise, cells were grown at 30°C in LB (0.5% NaCl) or in M9 minimal medium supplemented with 0.2% maltose, 0.2% casamino acids and 50 μg/ml L-tryptophan (M9-mal). When appropriate, the medium was supplemented with 50 μg/ml ampicillin (Amp), 50 μg/ml spectinomycin (Spec), 25 μg/ml kanamycin (Kan), 25 μg/ml chloramphenicol (Cam) or 12.5 μg/ml tetracycline (Tet). Amp and Cam concentrations were reduced to 15 and 10 μg/ml, respectively, when cells carried *bla* or *cat* integrated into the chromosome. Other details are specified in the text.

For BACTH analyses (Karimova *et al*, 1998), plasmid pairs encoding the indicated T18 and T25 fusions were co-transformed into BTH101 [*cya*-99], and individual colonies were patched on M9 agar containing 0.2% glucose, 50 μg/ml Amp, 25 μg/ml Kan, 40 μg/ml X-Gal and 250 μM IPTG. Plates were incubated at 30°C and inspected after 24, 30 and 36 h.

EZTnkan-2 (Epicentre) mutagenesis of strain TB28/pFB184 [Δ*lacIZYA*/P_{lac}::*sdiA*::*lacZ*], the subsequent screen for *rod* mutants and the mapping of insertions were carried out essentially as described (Bernhardt and de Boer, 2004). Complete details are provided as Supplementary data.

Microscopy

Live cells were imaged on 1.2% agarose pads made with either 0.5% NaCl (for LB cultures) or M9 salts (for M9 cultures). When indicated, cells were chemically fixed as described earlier (Bendezu and de Boer, 2008) and DAPI was added to 0.25 μg/ml, 2 min prior to imaging.

Microscopy set-ups are detailed further in Supplementary data.

Other methods

Measurements of cellular parameters and quantitative western blot analyses were carried out as before (Bendezu and de Boer, 2008). Details on the purification of antigens for antibody production are given as Supplementary data.

Supplementary data

Supplementary data are available at *The EMBO Journal* Online (http://www.embojournal.org).

Acknowledgements

We thank Yu-Ting Su and Elizabeth Zeng for help in plasmid construction; Stuart Austin, Daniel Ladant, Gouzel Karimova, Kenneth Marians, David McPheeters and Steven Sandler for materials, and Hironori Niki and Christine Jacobs-Wagner for communicating their independent discoveries of RodZ and for agreeing on its name. This study was supported by a Human Frontiers Science Program award (RGP0001/2003) and NIH GM57059 (to PAJdB), and NIH NRSA Institutional Training Grant T32GM08056 (to FOB). TGB holds a Career Award in the Biomedical Sciences from the Burroughs Wellcome Fund.

References

Bendezu FO, de Boer PA (2008) Conditional lethality, division defects, membrane involution, and endocytosis in *mre* and *mrd* shape mutants of *Escherichia coli*. *J Bacteriol* **190:** 1792–1811

Bernhardt TG, de Boer PA (2004) Screening for synthetic lethal mutants in *Escherichia coli* and identification of EnvC (YibP) as a periplasmic septal ring factor with murein hydrolase activity. *Mol Microbiol* **52:** 1255–1269

Cabeen MT, Jacobs-Wagner C (2007) Skin and bones: the bacterial cytoskeleton, cell wall, and cell morphogenesis. *J Cell Biol* **179:** 381–387

Carballido-Lopez R, Formstone A, Li Y, Ehrlich SD, Noirot P, Errington J (2006) Actin homolog MreBH governs cell morphogenesis by localization of the cell wall hydrolase LytE. *Dev Cell* **11:** 399–409

Daniel RA, Errington J (2003) Control of cell morphogenesis in bacteria: two distinct ways to make a rod-shaped cell. *Cell* **113:** 767–776

de Pedro MA, Donachie WD, Höltje JV, Schwarz H (2001) Constitutive septal murein synthesis in *Escherichia coli* with impaired activity of the morphogenetic proteins RodA and penicillin-binding protein 2. *J Bacteriol* **183:** 4115–4126

den Blaauwen T, Aarsman ME, Vischer NO, Nanninga N (2003) Penicillin-binding protein PBP2 of *Escherichia coli* localizes preferentially in the lateral wall and at mid-cell in comparison with the old cell pole. *Mol Microbiol* **47:** 539–547

den Blaauwen T, de Pedro MA, Nguyen-Disteche M, Ayala JA (2008) Morphogenesis of rod-shaped sacculi. *FEMS Microbiol Rev* **32:** 321–344

Divakaruni AV, Baida C, White CL, Gober JW (2007) The cell shape proteins MreB and MreC control cell morphogenesis by positioning cell wall synthetic complexes. *Mol Microbiol* **66:** 174–188

Divakaruni AV, Loo RR, Xie Y, Loo JA, Gober JW (2005) The cell-shape protein MreC interacts with extracytoplasmic proteins including cell wall assembly complexes in *Caulobacter crescentus*. *Proc Natl Acad Sci USA* **102:** 18602–18607

Dye NA, Pincus Z, Theriot JA, Shapiro L, Gitai Z (2005) Two independent spiral structures control cell shape in *Caulobacter*. *Proc Natl Acad Sci USA* **102:** 18608–18613

Figge RM, Divakaruni AV, Gober JW (2004) MreB, the cell shape-determining bacterial actin homologue, co-ordinates cell wall morphogenesis in *Caulobacter crescentus*. *Mol Microbiol* **51:** 1321–1332

Formstone A, Errington J (2005) A magnesium-dependent *mreB* null mutant: implications for the role of *mreB* in *Bacillus subtilis*. *Mol Microbiol* **55:** 1646–1657

Gerdes SY, Scholle MD, Campbell JW, Balazsi G, Ravasz E, Daugherty MD, Somera AL, Kyrpides NC, Anderson I, Gelfand MS, Bhattacharya A, Kapatral V, D'Souza M, Baev MV, Grechkin Y, Mseeh F, Fonstein MY, Overbeek R, Barabasi AL, Oltvai ZN *et al* (2003) Experimental determination and system level analysis of essential genes in *Escherichia coli* MG1655. *J Bacteriol* **185:** 5673–5684

Gitai Z, Dye NA, Reisenauer A, Wachi M, Shapiro L (2005) MreB actin-mediated segregation of a specific region of a bacterial chromosome. *Cell* **120:** 329–341

Guzman LM, Weiss DS, Beckwith J (1997) Domain-swapping analysis of FtsI, FtsL, and FtsQ, bitopic membrane proteins essential for cell division in *Escherichia coli*. *J Bacteriol* **179:** 5094–5103

Haldimann A, Wanner BL (2001) Conditional-replication, integration, excision, and retrieval plasmid-host systems for gene structure–function studies of bacteria. *J Bacteriol* **183:** 6384–6393

Hecht S, Eisenreich W, Adam P, Amslinger S, Kis K, Bacher A, Arigoni D, Rohdich F (2001) Studies on the nonmevalonate pathway to terpenes: the role of the GcpE (IspG) protein. *Proc Natl Acad Sci USA* **98:** 14837–14842

Hu B, Yang G, Zhao W, Zhang Y, Zhao J (2007) MreB is important for cell shape but not for chromosome segregation of the filamentous cyanobacterium *Anabaena* sp. PCC 7120. *Mol Microbiol* **63:** 1640–1652

Ishino F, Park W, Tomioka S, Tamaki S, Takase I, Kunugita K, Matsuzawa H, Asoh S, Ohta T, Spratt BG, Matsuhashi M (1986) Peptidoglycan synthetic activities in membranes of *Escherichia coli* caused by overproduction of penicillin-binding protein 2 and RodA protein. *J Biol Chem* **261:** 7024–7031

Jones LJ, Carballido-Lopez R, Errington J (2001) Control of cell shape in bacteria: helical, actin-like filaments in *Bacillus subtilis*. *Cell* **104:** 913–922

Karczmarek A, Martinez-Arteaga R, Alexeeva S, Hansen FG, Vicente M, Nanninga N, den Blaauwen T (2007) DNA and origin region segregation are not affected by the transition from rod to sphere after inhibition of *Escherichia coli* MreB by A22. *Mol Microbiol* **65:** 51–63

Karimova G, Pidoux J, Ullmann A, Ladant D (1998) A bacterial two-hybrid system based on a reconstituted signal transduction pathway. *Proc Natl Acad Sci USA* **95:** 5752–5756

Kruse T, Blagoev B, Lobner-Olesen A, Wachi M, Sasaki K, Iwai N, Mann M, Gerdes K (2006) Actin homolog MreB and RNA polymerase interact and are both required for chromosome segregation in *Escherichia coli*. *Genes Dev* **20:** 113–124

Kruse T, Bork-Jensen J, Gerdes K (2005) The morphogenetic MreBCD proteins of *Escherichia coli* form an essential membrane-bound complex. *Mol Microbiol* **55:** 78–89

Kruse T, Moller-Jensen J, Lobner-Olesen A, Gerdes K (2003) Dysfunctional MreB inhibits chromosome segregation in *Escherichia coli*. *EMBO J* **22:** 5283–5292

Leaver M, Errington J (2005) Roles for MreC and MreD proteins in helical growth of the cylindrical cell wall in *Bacillus subtilis*. *Mol Microbiol* **57:** 1196–1209

Newitt JA, Ulbrandt ND, Bernstein HD (1999) The structure of multiple polypeptide domains determines the signal recognition particle targeting requirement of *Escherichia coli* inner membrane proteins. *J Bacteriol* **181:** 4561–4567

Pollard TD (2007) Regulation of actin filament assembly by Arp2/3 complex and formins. *Annu Rev Biophys Biomol Struct* **36:** 451–477

Shih YL, Le T, Rothfield L (2003) Division site selection in *Escherichia coli* involves dynamic redistribution of Min proteins within coiled structures that extend between the two cell poles. *Proc Natl Acad Sci USA* **100:** 7865–7870

Shih YL, Rothfield L (2006) The bacterial cytoskeleton. *Microbiol Mol Biol Rev* **70:** 729–754

Shiomi D, Sakai M, Niki H (2008) Determination of bacterial rod shape by a novel cytoskeletal membrane protein. *EMBO J* **27:** 3081–3091

Soufo HJ, Graumann PL (2003) Actin-like proteins MreB and Mbl from *Bacillus subtilis* are required for bipolar positioning of replication origins. *Curr Biol* **13:** 1916–1920

Spratt BG (1975) Distinct penicillin binding proteins involved in the division, elongation, and shape of *Escherichia coli* K12. *Proc Natl Acad Sci USA* **72:** 2999–3003

Srivastava P, Demarre G, Karpova TS, McNally J, Chattoraj DK (2007) Changes in nucleoid morphology and origin localization upon inhibition or alteration of the actin homolog, MreB, of *Vibrio cholerae*. *J Bacteriol* **189:** 7450–7463

Tamaki S, Matsuzawa H, Matsuhashi M (1980) Cluster of *mrdA* and *mrdB* genes responsible for the rod shape and mecillinam sensitivity of *Escherichia coli*. *J Bacteriol* **141:** 52–57

Tatusov RL, Fedorova ND, Jackson JD, Jacobs AR, Kiryutin B, Koonin EV, Krylov DM, Mazumder R, Mekhedov SL, Nikolskaya AN, Rao BS, Smirnov S, Sverdlov AV, Vasudevan S, Wolf YI, Yin JJ, Natale DA (2003) The COG database: an updated version includes eukaryotes. *BMC Bioinformatics* **4:** 41

Tiyanont K, Doan T, Lazarus MB, Fang X, Rudner DZ, Walker S (2006) Imaging peptidoglycan biosynthesis in *Bacillus subtilis* with fluorescent antibiotics. *Proc Natl Acad Sci USA* **103:** 11033–11038

van den Ent F, Amos LA, Lowe J (2001) Prokaryotic origin of the actin cytoskeleton. *Nature* **413:** 39–44

van den Ent F, Leaver M, Bendezu F, Errington J, de Boer P, Lowe J (2006) Dimeric structure of the cell shape protein MreC and its functional implications. *Mol Microbiol* **62:** 1631–1642

Varma A, de Pedro MA, Young KD (2007) FtsZ directs a second mode of peptidoglycan synthesis in *Escherichia coli*. *J Bacteriol* **189:** 5692–5704

Vinella D, Joseleau-Petit D, Thevenet D, Bouloc P, D'Ari R (1993) Penicillin-binding protein 2 inactivation in *Escherichia coli* results in cell division inhibition, which is relieved by FtsZ overexpression. *J Bacteriol* **175:** 6704–6710

Vollmer W, Bertsche U (2008) Murein (peptidoglycan) structure, architecture and biosynthesis in *Escherichia coli*. *Biochim Biophys Acta* **1778:** 1714–1734

Wachi M, Doi M, Okada Y, Matsuhashi M (1989) New *mre* genes *mreC* and *mreD*, responsible for formation of the rod shape of *Escherichia coli* cell. *J Bacteriol* **171:** 6511–6516

Wachi M, Doi M, Tamaki S, Park W, Nakajima-lijima S, Matsuhashi M (1987) Mutant isolation and molecular cloning of *mre* genes, which determine cell shape, sensitivity to mecillinam, and amount of penicillin-binding proteins in *Escherichia coli*. *J Bacteriol* **169:** 4935–4940

Wachi M, Matsuhashi M (1989) Negative control of cell division by *mreB*, a gene that functions in determining the rod shape of *Escherichia coli* cells. *J Bacteriol* **171:** 3123–3127

Wyche JH, Kennedy J, Hartman Z, Hartman PE, Diven J (1974) Round-cell mutant of *Salmonella typhimurium*. *J Bacteriol* **120:** 965–969

